RSC Advances

PAPER

View Article Online
View Journal | View Issue

Mesoporous C, N-codoped TiO_2 hybrid shells with enhanced visible light photocatalytic performance†

Cite this: RSC Adv., 2017, 7, 15513

Minggui Wang, Jie Han,* Yimin Hu and Rong Guo*

Received 23rd January 2017
Accepted 2nd March 2017

DOI: 10.1039/c7ra00985b

rsc.li/rsc-advances

Mesoporous C, N-codoped TiO_2 (C/N-TiO_2) hybrid shells incorporated with graphite carbon were synthesized using polystyrene spheres as templates, followed by polyaniline (PANI) and TiO_2 coating, and then post-treatments of etching and calcination, where PANI functioned as both C and N doping sources and supplied the graphite carbon. Compared with pure TiO_2 and C-doped TiO_2 (C-TiO_2) hybrid shells, C/N-TiO_2 hybrid shells exhibited enhanced photocatalytic activity in the degradation of organic dyes and H_2 production under visible light irradiation, which could be attributed to the enhanced visible light absorption and charge separation efficiency associated with the codoped-C and N and the presence of graphite carbon. It is believed that the strategy presented here will provide a promising route for the construction of other C/N-semiconductor hybrid shells for broader applications.

Introduction

Titania (TiO_2), as one of the photocatalysts with the most potential, has been widely investigated for energy storage and environmental treatment,[1] owing to its low cost, non-toxicity, stability and high photocatalytic activity.[2] However, the photocatalytic activity of pure TiO_2 is still very low, mainly due to its relatively large band gap which can only be excited by UV light and the high rate of recombination of photogenerated electron–hole pairs.[3] To solve these problems, many effective strategies have been made to improve the photocatalytic activity by enhancing its visible light absorption and improving the separation efficiency of electron–hole pairs.[4] One common approach for shifting the light absorption of TiO_2 to the visible region is to change its inner band structure by replacing the oxygen in the lattice to narrow the band gap. Recently, efforts have been focused on introducing non-metallic elements into TiO_2 to enhance its photocatalytic activity (such as C, N, S, B and F).[5] It has been reported that the introduction of these non-metallic elements can shift the light absorption of TiO_2 to the visible light region to enhance the visible light absorption and corresponding photocatalytic activity. Among these non-metallic elements-doped TiO_2 materials, C or N-doped TiO_2-based composites have attracted increasing attention in particular. In the process of C doping, C element can produce a hybrid orbital over the valence band of TiO_2 to decrease the band gap with enhanced visible light absorption.[6] As for N doping, it has been reported that doped N can act as trapping centers for photogenerated electrons and effectively suppresses the recombination rate of the photogenerated electrons and holes.[7] Although many studies have been focused on the preparation of C or N-doped TiO_2, however, little work has done on the construction of C, N-codoped TiO_2 (C/N-TiO_2). It is believed that C/N-TiO_2 will be of highly interest because it possesses both enhanced visible light absorption and separation efficiency of electron–hole pairs, which can contribute to improved photocatalytic activity.

Polyaniline, as one of the most promising conducting polymers, has been widely studied due to its low cost, ease preparation, high environmental stability, and novel special structure-related properties.[8] It involves both N and C elements with relatively high molar ratio of N to C at 1/6, which can be chosen as the potential doping source for N and C codoping in TiO_2 within a one-step process. More importantly, in comparison with commonly used gaseous dopants, such as NH_3,[9] PANI is economical, and can be fully utilized during the doping process with the additional graphite carbon acts as electrically conductive components to improve the transmission of photogenerated electrons.[10] Therefore, designed-synthesis of C/N-TiO_2 hybrids as powerful photocatalysis using PANI as doping sources is of highly important.

Herein, mesoporous C/N-TiO_2 hybrid shells have been successfully fabricated through *in situ* polymerization and sol–gel coating method. The calcination route is applied to synthesize C/N-TiO_2 hybrid shells where PANI functions as both C and N doping sources and supplies the graphite carbon, which help to improve the visible light absorption and photogenerated electron–hole pair separation efficiency of TiO_2, and finally lead to enhanced photocatalytic activity. To the best of our knowledge, this is the first report of one step C, N-codoping of TiO_2 using PANI as the dopant. Results from catalytic investigations of C/N-TiO_2 hybrid shells toward the degradation

---

School of Chemistry and Chemical Engineering, Yangzhou University, Yangzhou, Jiangsu, 225002, P. R. China. E-mail: hanjie@yzu.edu.cn; guorong@yzu.edu.cn

† Electronic supplementary information (ESI) available: Additional TEM, XPS, fluorescence spectra and photocatalytic results towards RhB degradation of C/N-TiO_2 photocatalysts. See DOI: 10.1039/c7ra00985b

of organic pollutions and H_2 production under visible light irradiation indicate that C and N codoping can remarkably improve the photocatalytic performance of TiO_2. The superior photocatalytic performance of C/N-TiO_2 hybrid shells clearly indicates their potential as low-cost but powerful visible light photocatalysts.

Experimental

Materials

Tetrabutyl orthotitanate (TBOT, 97%) was obtained from Fluka. Anhydrous ethanol, rhodamine B (RhB), ammonia (25–28%), hydrochloric acid (HCl), acetonitrile, styrene monomer, methacrylic acid, ammonium persulfate (APS), and all other reagents were obtained from Sinopharm Chemical Reagent Co. Ltd. (China). Aniline monomer was distilled under reduced pressure. The water used in this study was deionized and purified through a Millipore system.

Synthesis of polystyrene (PS) nanoparticles

In a typical synthesis, styrene monomer (35.0 mL) was mixed with deionized water (150.0 mL), methacrylic acid (1.0 mL) and an aqueous solution of APS (1.0 mL H_2O containing 0.1575 g APS). After stirring for 3 h under 95 °C, the PS nanoparticles were separated by centrifugation, washed three times with ethanol, and then dried under vacuum at 50 °C for 6 h.

Synthesis of PS/PANI core/shell hybrids

In typical, 111.4 μL aniline was added to 15.0 mL water at ice bath and under ultrasonic treatment for 15 min, followed by the addition of the 0.568 g PS. The mixture was stirred with ultrasonic assistance for 30 min at ice bath. Then 7.0 mL APS aqueous solution (0.045 g mL^{-1}) was added to the dispersion. After stirring for 5 min, an aqueous solution of HCl (1.4 mL H_2O containing 114.8 μL HCl) solution was slowly added. After stirring for 4 h at ice bath, the particles were isolated by centrifugation and washed with ethanol, and then dried in an oven at 80 °C for 6 h.

Synthesis of mesoporous C/N-TiO_2 hybrid shells

In typical, 20.0 mg of as-prepared PS/PANI hybrids were dispersed in a mixture of ethanol (25.0 mL) and acetonitrile (7.0 mL) under vigorous stirring. After adding ammonia aqueous solution (0.2 mL), TBOT (0.4 mL) in a mixture of ethanol (3.0 mL) and acetonitrile (1.0 mL) was injected into the mixture. After stirring for 3 h, the PS/PANI/TiO_2 hybrids were isolated by centrifugation and washed with ethanol, and then dispersed in 20.0 mL tetrahydrofuran (THF) under vigorous stirring for 5 h to completely remove the PS template, the PANI/TiO_2 hybrids were isolated by centrifugation and washed with ethanol, and then dried in an oven at 80 °C for 6 h. After that, the PANI/TiO_2 hybrids were calcined under N_2 protection at different temperature (500–800 °C) for 4 h to crystallize TiO_2, and carbonize PANI through pyrolysis. By controlling the calcination temperature at 500, 600, 700, and 800 °C, the as-prepared C/N-TiO_2 hybrid shells were denoted as C/N-TiO_2(500), C/N-TiO_2(600), C/N-TiO_2(700), and C/N-TiO_2(800), respectively.

Synthesis of pure TiO_2 and C-TiO_2 hybrid shells

In typical, 15.0 mg PS nanoparticles were dispersed in a mixture of ethanol (25.0 mL) and acetonitrile (7.0 mL) under vigorous stirring. After adding ammonia aqueous solution (0.2 mL), TBOT (0.4 mL) in a mixture of ethanol (3.0 mL) and acetonitrile (1.0 mL) was injected into the mixture. After stirring for 3 h, the particles were isolated by centrifugation and washed with water, and then dried in an oven at 80 °C for 6 h. After that, the PS/TiO_2 core/shell hybrids were calcined under air and N_2 protection at 600 °C for 4 h to produce TiO_2(600) and C-TiO_2(600).

Photocatalytic activity tests

(1) Photocatalytic pollute degradation. The photocatalytic activity of the C/N-TiO_2 hybrid shells was firstly investigated in degradation of organic pollutes (RhB and phenol). In a typical photocatalytic degradation experiment, 5.0 mg catalyst was dispersed in 25.0 mL RhB aqueous solution (2.0×10^{-5} mol L^{-1}) or 25.0 mL phenol aqueous solution (10 mg L^{-1}) in a quartz cell and then stirred in dark for 30 min to ensure equilibrium adsorption. The light sources of the visible lamp (400 W metal halide) with a 400 nm filter were used in a commercial photoreactor system (Xujiang XPA-7). The concentration of organic pollutes was measured with a UV-vis spectrophotometer (HR2000CG-UV-NIR, Ocean Optics).

(2) Photocatalytic H_2 production. In a typical run of photocatalytic H_2 production, 10.0 mg catalyst was dispersed in 10.0 mL of solution containing water and methanol (with volume ratio of water to methanol fixed at 3) under stirring for 20 min, bubbled with nitrogen for 30 min to remove the dissolved oxygen, and then sealed with a parafilm. The suspension was irradiated under stirring with a Xe light source (350 W) at power density 100 mW cm^{-2}. The visible light was filtered with a UV-cutoff filter (400 nm). The photocatalytic system was maintained at room temperature. The gas produced were periodically withdrawn with a syringe and examined by a gas chromatography (GC). The quantum efficiency (QE) was calculated according to the following equation:

$$\mathrm{QE}\ [\%] = \frac{\text{number of reacted electrons}}{\text{number of incident photons}} \times 100\%$$

Characterization

Morphologies were characterized with a transmission electron microscopy (TEM, JEM-2100) and a high-resolution TEM (HRTEM, Tecnai G2 F30 S-Twin TEM, FEI). The crystal phase was analyzed by XRD using a Bruker AXS D8 ADVANCE X-ray diffractometer. The specific surface and pore size were studied by using a Beishide 3H-2000PS2 analysis instrument. UV/Vis diffuse reflectance spectra (Cary 5000, Varian) was used to test the optical properties. The phase composition was measured using an Axis Ultra X-ray photoelectron spectroscope (XPS, Kratos Analytical Ltd., UK) equipped with a standard monochromatic Al Kα source ($h\nu$ = 1486.6 eV).

Photoluminescence (PL) spectra were measured using a fluorescence spectrophotometer (Hitachi F-7000), and the excitation wavelength was 315 nm. The total organic carbon (TOC) values of RhB solution were determined using a total organic carbon analyzer (Elementar vario TOC). The oxygen vacancies of the as-prepared samples were studied by electron paramagnetic resonance (EPR) measurements (A300-10/12, Bruker).

Results and discussion

Scheme 1 illustrates the procedures for preparing mesoporous C/N-TiO_2 hybrid shells. Specifically, PS nanospheres were used as templates, loaded sequentially with layers of PANI and TiO_2 by *in situ* polymerization and sol–gel methods, respectively. Finally, the PS templates were removed and then PANI/TiO_2 hybrid shells are calcined under N_2 atmosphere, leading to the formation of C/N-TiO_2 hybrid shells.

Fig. S1† shows the morphology evolution from PS templates to PS/PANI/TiO_2 hybrids. Fig. 1a and b present the typical low and high magnified TEM images of C/N-TiO_2(600) hybrid shells, where the shell thickness is ~40 nm, and the particle size distribution of C/N-TiO_2(600) hybrid shells from a statistical study of the TEM images was given in Fig. S2.† The HRTEM image (Fig. 1c) indicates that the lattice fringes of 0.35 nm match the plane of anatase TiO_2 (101). The hollow structure of C/N-TiO_2(600) hybrid shells can be further confirmed by high-angle annular dark-field scanning transmission electron microscope (HAADF-STEM), as shown in Fig. 1d. The corresponding energy dispersive X-ray spectroscopic (EDS) mapping of C, N and Ti are shown in Fig. 1e–g, indicating the homogeneous distribution of C and N elements in TiO_2 shell.

The calcination temperature is found to affect the morphology of C/N-TiO_2 hybrid shells. As shown in Fig. 2, it can be clearly found that the final hollow structure can be well maintained at the calcination temperature below 700 °C. When the calcination temperature reaches 800 °C, the hybrid shells are aggregated and the shell grains are grown into big particles.

In order to clarify the C/N codoping effect, pure TiO_2 and C-TiO_2 hybrid shells were also synthesized using a similar strategy. As started from PS which only contains C element, TiO_2 shell is then coated on surfaces of PS, followed by calcination under N_2 atmosphere, leading to the formation of C-TiO_2 hybrid shells. If the calcination is placed under air condition, carbon can be completely removed and then pure TiO_2 hollow spheres can be obtained. Fig. S3† gives the typical TEM images of pure TiO_2(600) hollow spheres and C-TiO_2(600) hybrid shells. It can be seen that pure TiO_2(600) hollow spheres maintains the hollow structure but with some broken shells, whereas C-TiO_2(600) can maintain the complete hollow structures. The tenacity of doped TiO_2 hybrid shells (Fig. 1 and S1b†) is obviously superior to that of undoped TiO_2 hybrid shells (Fig. S1a†), which may be attributed to the presence of graphite carbon resulted from PANI carbonization (as confirmed later by Raman spectra) that bridges TiO_2 crystalline grains and improves the shell integrity.

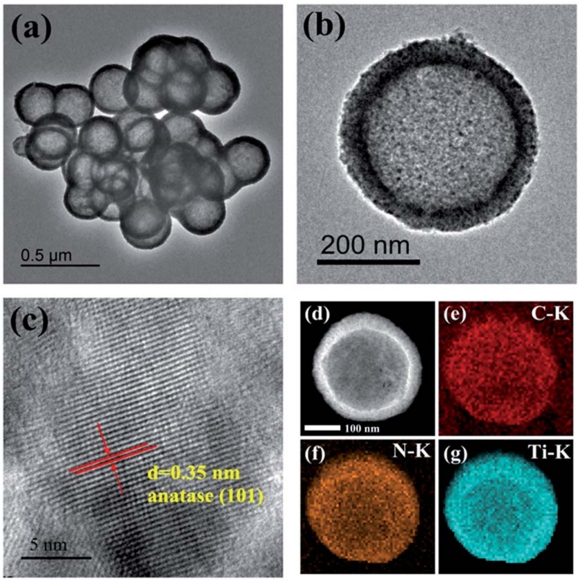

Fig. 1 (a, b) TEM and (c) HRTEM images of C/N-TiO_2(600) hybrid shells. (d) HAADF-STEM image of C/N-TiO_2(600) hybrid shells and (e–g) EDS maps of (e) C, (f) N, and (g) Ti from a single C/N-TiO_2(600) particle given in (d).

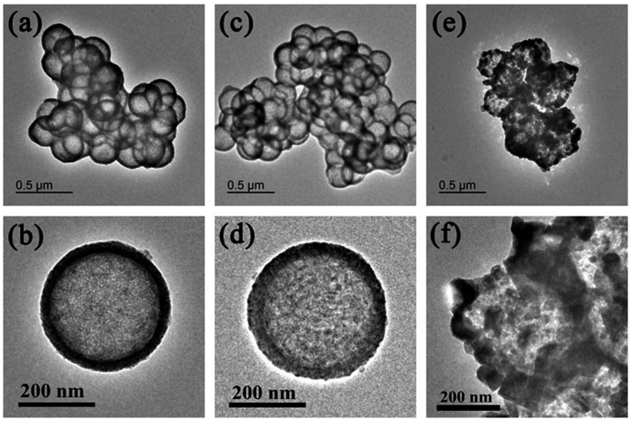

Fig. 2 TEM images of (a, b) C/N-TiO_2(500), (c, d) C/N-TiO_2(700), and (e, f) C/N-TiO_2(800) hybrid shells.

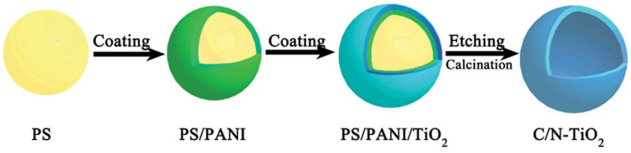

Scheme 1 Schematic representation of the synthesis processes of C/N-TiO_2 hybrid shells.

The chemical composition and element valence of C/N-TiO_2(600) hybrid shells as studied by XPS analysis are shown in Fig. 3. The XPS survey spectrum (Fig. 3a) of C/N-TiO_2(600) hybrid shells indicates the presence of Ti, C, O and N elements. The C 1s spectrum of C/N-TiO_2(600) hybrid shells are shown in Fig. 3b. The peaks at 284.8, 285.9, 287.0, and 288.9 eV are ascribed to the binding energy of sp2 C–C, C–N, C=N and C–O–

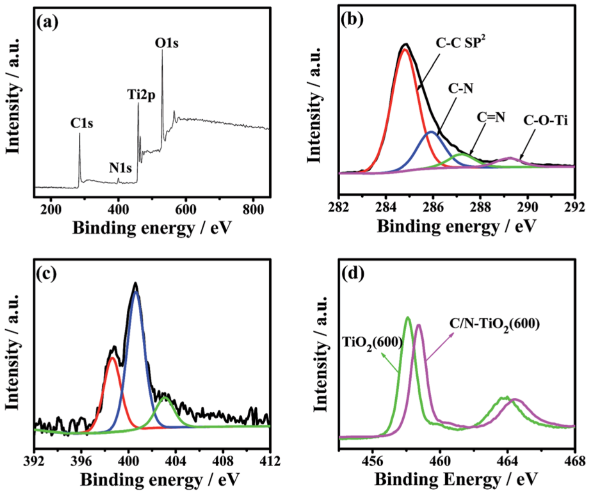

Fig. 3 (a) The survey, (b) C 1s and (c) N 1s XPS spectra of C/N-TiO_2(600) hybrid shells. (d) Ti 2p XPS spectra of pure TiO_2(600) hollow spheres and C/N-TiO_2(600) hybrid shells.

Ti bonds, respectively. The N 1s spectra of C/N-TiO_2(600) hybrid shells (Fig. 3c) can be attributed to pyridine N (398.3 eV), quaternary N (400.6 eV) and oxidized N (403.0 eV). Results indicate the successful C/N cooping in TiO_2.[11] Fig. 3d is the high resolution Ti 2p spectra of pure TiO_2(600) hollow spheres and C/N-TiO_2(600) hybrid shells. It can be seen that TiO_2 hybrid shells show two peaks at 458.1 and 463.8 eV, which contribute to the binding energies of Ti $2p_{3/2}$ and Ti $2p_{1/2}$ levels, respectively, indicating a normal state of Ti^{4+}.[12] In addition, in contrast to pure TiO_2(600) hollow spheres, the Ti 2p binding energy of C/N-TiO_2(600) hybrid shells shifts toward high energy, which may be attributed to the C/N codoping in TiO_2.

In addition, the electron paramagnetic resonance (EPR) was also used to investigate the oxygen vacancies in the samples. As shown in Fig. 4a, the pure TiO_2(600) hollow spheres, C-TiO_2(600) and C/N-TiO_2(600) hybrid shells show a resonance at about $g = 2.000$, which is attributed to the signal of oxygen vacancy. It has been reported that the stronger peak intensity of EPR spectra suggesting the higher existing oxygen vacancy.[13] Moreover, it can be seen from Fig. 4a that the signal intensity of oxygen vacancy increased with the doping of the C and N into TiO_2, indicating an increased concentration of oxygen vacancy in C-TiO_2(600) and C/N-TiO_2(600) samples. The more oxygen vacancies indicate the higher degree of doping.

The phase structures of pure TiO_2(600) hollow spheres, C-TiO_2(600) and C/N-TiO_2(600) hybrid shells were investigated by XRD analysis and the results were presented in Fig. 4b. Most of the identified peaks for TiO_2 are assigned to anatase (JCPDS, no. 73-1764). However, it also can be observed that a small rutile diffraction peak at 27.5° in pure TiO_2(600) hollow spheres and C-TiO_2(600) hybrid shells, suggesting the presence of rutile phase. Notably, as for C/N-TiO_2 hybrid shells, the intensity and sharpness of the XRD peaks are strengthened with increasing calcination temperature, suggesting increased crystallinity of TiO_2 grains. When the calcination temperature reaches above 700 °C, such as C/N-TiO_2(800), rutile phase TiO_2 is the dominating phase.

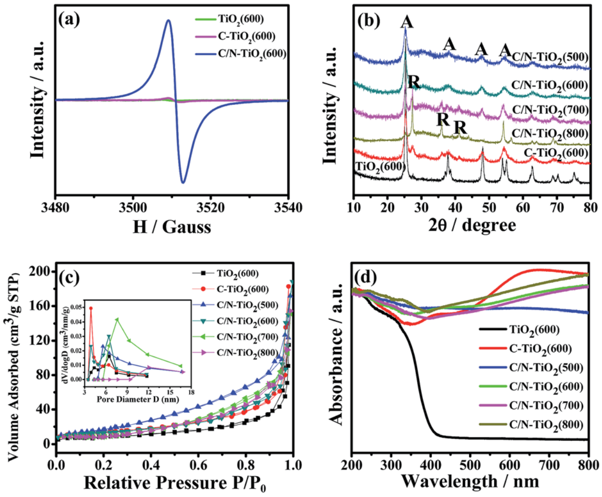

Fig. 4 (a) EPR spectra of pure TiO_2(600) hollow spheres, C-TiO_2(600) and C/N-TiO_2(600) hybrid shells. (b) XRD patterns, (c) nitrogen adsorption–desorption isotherms and (d) UV/Vis diffused reflectance spectra of pure TiO_2(600) hollow spheres, C-TiO_2(600) and C/N-TiO_2 hybrid shells. Inset in (c) is the corresponding pore size distribution.

The specific surface area and pore structure of pure TiO_2(600) hollow spheres, C-TiO_2(600) and C/N-TiO_2 hybrid shells were characterized by N_2 adsorption–desorption analysis. It has been reported that the high specific surface areas can favor increased photocatalytic activity.[14] Fig. 4c displays N_2 adsorption–desorption isotherms and their corresponding pore size distribution curves. It can be seen that all samples showed similar sorption isotherms and pore size distributions. The corresponding specific surface area, pore volume and pore size of different samples are summarized in Table 1. It can be found that the C/N-TiO_2(600) hybrid shells have the highest BET surface area and pore volume, which are believed to provide more active sites as photocatalysts.

UV/Vis diffuse reflectance spectroscopy was further used to investigate the optical properties of as-prepared samples. The UV/Vis diffuse reflectance spectra of pure TiO_2(600) hollow spheres, C-TiO_2(600) and C/N-TiO_2 hybrid shells were shown in Fig. 4d. The absorption band near 400 nm is ascribed to the band-edge absorption of anatase TiO_2.[15] With the introduction of carbonized PS or PANI, the powder changes from white to black. In comparison with pure TiO_2(600) hollow spheres, the

Table 1 BET surface area and BJH pore size and volume of TiO_2(600), C-TiO_2(600) and C/N-TiO_2 hybrid shells

Catalysts	Surface area (m^2 g^{-1})	Pore size (nm)	Pore volume (cm^3 g^{-1})
TiO_2(600)	89.8	5.1	0.20
C-TiO_2(600)	108.3	3.7	0.32
C/N-TiO_2(500)	119.1	5.2	0.30
C/N-TiO_2(600)	125.5	6.1	0.54
C/N-TiO_2(700)	102.9	8.4	0.27
C/N-TiO_2(800)	95.8	10.4	0.53

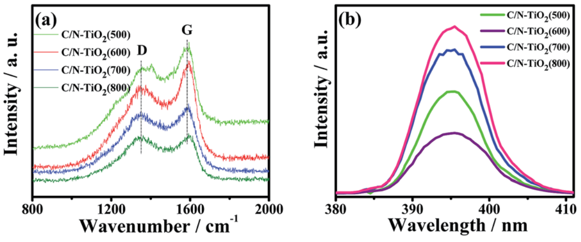

Fig. 5 (a) Raman and (b) PL spectra of C/N-TiO$_2$ hybrid shells.

absorption edges of C-TiO$_2$(600) and C/N-TiO$_2$(600) hybrid shells are found to shift towards the visible light region, and the C/N-TiO$_2$ hybrid shells exhibit enhanced visible light absorption with increasing calcination temperature. It is believed that the broad absorption in visible light region will enhance the effective utilization of solar energy.

Fig. 5a shows the Raman scattering spectra of C/N-TiO$_2$ hybrid shells. The two characteristic peaks at about 1360 cm^{-1} (D band) and 1580 cm^{-1} (G band) for the graphite carbon can be clearly found, indicating the well degree of carbonization from PANI polymer to graphite carbon.[16] The D/G intensity ratios for C/N-TiO$_2$ hybrid shells increase with calcination temperature, suggesting increased carbonization degree.

It has been reported that the PL emission can be caused by the recombination of electron–hole pairs of photocatalysts, and the smaller PL intensity suggesting the lower recombination rate of electron–hole pairs.[17] Fig. S4† shows the PL spectra of pure TiO$_2$(600) hollow spheres, C-TiO$_2$(600) and C/N-TiO$_2$(600) hybrid shells excited at 360 nm. It can be obviously seen that pure TiO$_2$(600) hollow spheres have a high intensity emission peak at around 395 nm, whereas the intensity decreases for C-TiO$_2$(600) hybrid shells, and weakens a lot for C/N-TiO$_2$(600) hybrid shells. Fig. 5b shows the PL spectra of C/N-TiO$_2$ hybrid shells. It is observed that the PL intensity of C/N-TiO$_2$(600) hybrid shells displays the lowest PL intensity in comparison with others. The results indicate that the recombination of photogenerated electron–hole pairs is effectively suppressed due to the codoping of C and N. The electrically conductive graphite carbon in C-TiO$_2$(600) hybrid shells is beneficial for electron transmission, and the introduction of N in C/N-TiO$_2$ hybrid shells can act as trapping centers for photogenerated electrons which further enhance the separation efficiency of electron–hole pairs.

The photocatalytic activities of pure TiO$_2$(600) hollow spheres, C-TiO$_2$(600) and C/N-TiO$_2$ hybrid shells were evaluated by the degradation of organic pollutions RhB and phenol under visible light irradiation. The photocatalytic activity of samples was firstly evaluated by monitoring the degradation of RhB under visible light irradiation. In order to make the as-prepared samples more comparable, the carbon content in C/N-TiO$_2$(600) hybrid shells was maintained similar to that in the C-TiO$_2$(600) hybrid shells by controlling the amount of PANI coating, which was measured by elementary analysis and the results were given in Table S1.† As shown in Fig. 6a and b, the degradation efficiency of RhB reaches 90% and 72% within 100 min for C/N-TiO$_2$(600) and C-TiO$_2$(600) hybrid shells, respectively. However, pure TiO$_2$(600) hollow spheres can convert only about 35%. The apparent reaction rate for C/N-TiO$_2$(600) ($k = 0.022$ min^{-1}) and C-TiO$_2$(600) hybrid shells ($k = 0.014$ min^{-1}) are 5.0 and 3.2 times higher than that for pure TiO$_2$(600) hollow spheres ($k = 0.0044$ min^{-1}), respectively. The photocatalytic results confirm that the incorporation of C and N into TiO$_2$ can significantly enhance their photocatalytic activities. Fig. 7a and b shows the results of RhB degradation using C/N-TiO$_2$ hybrid shells. It is clearly observed that the photocatalytic activity of C/N-TiO$_2$(600) hybrid shells exhibits the best photocatalytic performance. The apparent quantum efficiency for C/N-TiO$_2$(600) hybrid shells photocatalyst is calculated to be 0.89%. The photocatalytic activities of C/N-TiO$_2$(600) hybrid shells are superior to the

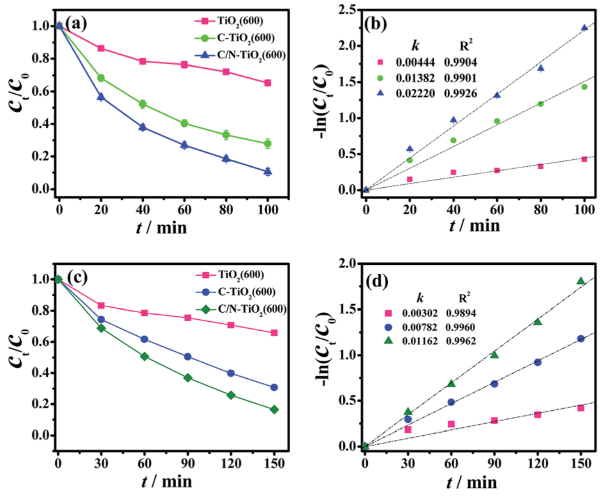

Fig. 6 Evolution of (a) RhB and (c) phenol concentration with reaction time and (b, d) their corresponding apparent reaction rates under visible light using pure TiO$_2$(600) hollow spheres, C-TiO$_2$(600) and C/N-TiO$_2$(600) hybrid shells as photocatalysts.

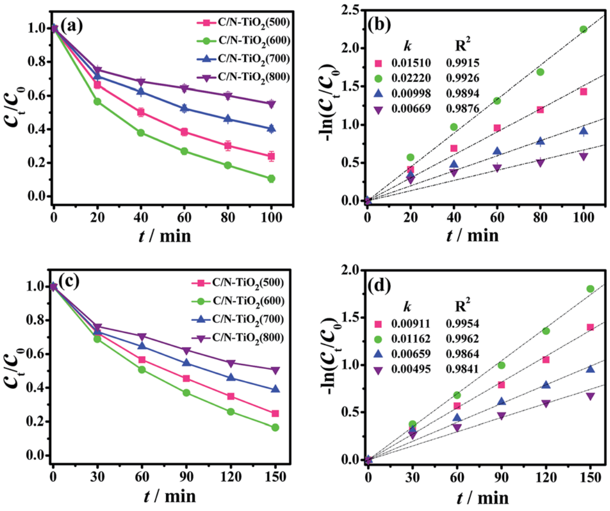

Fig. 7 Evolution of (a) RhB and (c) phenol concentration with reaction time and (b, d) their corresponding apparent reaction rates under visible light irradiation using C/N-TiO$_2$ hybrid shells as photocatalysts.

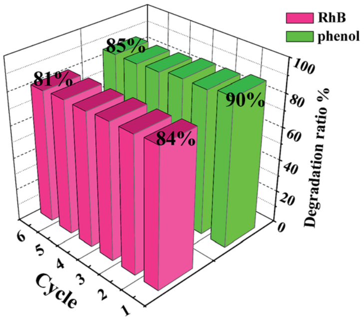

Fig. 8 Recyclability of C/N-TiO_2(600) hybrid shells as photocatalysts in degradation of RhB and phenol under visible light irradiation.

reported non-metallic element-doped TiO_2 hybrids in RhB degradation, as listed in Table S2.†

To further confirm the mineralization of RhB, changes in TOC values of RhB solution using C/N-TiO_2(600) hollow hybrids photocatalysts after visible light irradiation were detected (Fig. S5 and Table S3†). It can be seen that TOC removal proceeds much more slowly than the optical color change.[18] The decreasing in TOC values of RhB solution indicates that most RhB molecules were degraded into CO_2 after visible light irradiation in the presence of C/N-TiO_2(600) photocatalysts. As for degradation of phenol under visible light irradiation, C/N-TiO_2(600) hybrid shells also exhibited the highest photocatalytic activity as compared with pure TiO_2(600) hollow spheres and C-TiO_2(600) hybrid shells (Fig. 6c and d), where 84% of phenol was degraded within 150 min ($k = 0.012$ min^{-1}) with 0.56% apparent quantum efficiency. The photocatalytic activity of C/N-TiO_2 hybrid shells for phenol degradation follows the same order as degradation on RhB (Fig. 7c and d). In addition, the recyclability of the C/N-TiO_2 hollow hybrids has also been investigated. It can be seen that the photocatalytic activity of C/N-TiO_2 hybrid shells towards RhB and phenol degradation under visible light irradiation were slightly decayed after six consecutive runs (Fig. 8), but still had high photocatalytic performance, suggesting their high stability and recyclability.

Herein, the C/N-TiO_2 hybrid shells were also studied in photocatalytic H_2 production under visible light irradiation in methanol aqueous solution. Fig. 9a shows data for a photocatalytic activity comparison of pure TiO_2(600) hollow spheres, C-TiO_2(600) and C/N-TiO_2(600) hybrid shells in H_2 production. The highest H_2 production activity, as observed for C/N-TiO_2(600) hybrid shells, is about 291 μmol h^{-1} g^{-1} with 0.9% apparent quantum efficiency. Fig. 9b compares the photocatalytic activity of C/N-TiO_2 hybrid shells in H_2 production, which follows the same order as degradation on organic pollution. In addition, the activity sequences are the same if the photocatalytic activity is normalized to the specific surface area. The stability of C/N-TiO_2(600) hybrid shells in photocatalytic H_2 production was also studied, as presented in Fig. 9c. It can be seen that the C/N-TiO_2(600) hybrid shells can still exhibit high photocatalytic performance after five cycles. The C/N-TiO_2(600) hybrid shells can exhibit the best photocatalytic activity mainly owing to their well-defined hollow structure with high specific surface area, and appropriate anatase-rutile mixed phases.

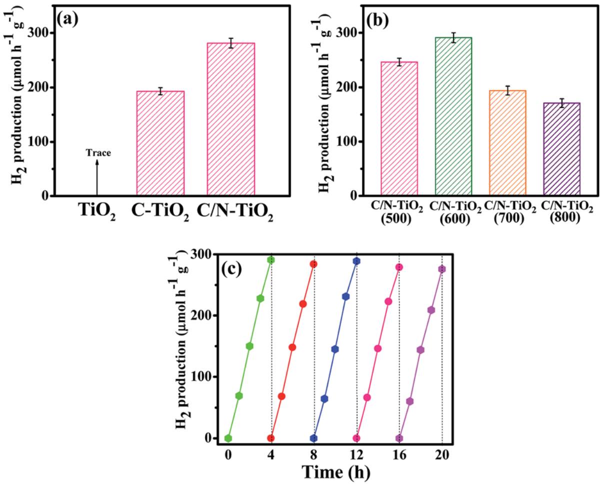

Fig. 9 Comparison of the photocatalytic production of H_2 (a) using TiO_2, C-TiO_2(600) and C/N-TiO_2(600) hybrid shells and (b) using C/N-TiO_2 hybrid shells as photocatalysts under visible light irradiation. (c) The recyclability of C/N-TiO_2(600) hybrid shells as photocatalysts in H_2 production under visible light irradiation.

Based on above analysis results, a possible mechanism of photocatalytic reaction under visible light irradiation over C/N-TiO_2 hybrid shells was proposed. When the C/N-TiO_2 hybrid shells were irradiated under visible light, VB electrons from TiO_2 could be excited due to the narrowed band gap of TiO_2 coming from C doping. In addition, the incorporation of graphite carbon in TiO_2 could facilitate the electron transmission, and the presence of N in C/N-TiO_2 hybrid shells could act as trapping centers for electrons. As a result, separation efficiency of electron–hole pairs could be greatly enhanced that leading to improved photocatalytic activity. During the photocatalytic process, the photogenerated electrons on the hybrid shells not only can be trapped by O_2, producing oxygen free radicals ($^{\bullet}O_2^{-}$), but also can reduce H^{+} ions to produce H_2. Meanwhile, the photogenerated holes can react with H_2O or hydroxide ions, producing hydroxyl radicals ($^{\bullet}OH$). Both oxygen free radicals and hydroxyl radicals are the powerful oxidizing species for organic pollution degradation. The generated $^{\bullet}OH$ radicals during the photocatalytic reactions under visible light are detected by using fluorescence method using terephthalic acid as a probe molecule, which can react with $^{\bullet}OH$ to produce a fluorescent substance.[19] Fig. 10a shows the change of fluorescence spectra with irradiation time under visible light irradiation, indicating $^{\bullet}OH$ generation for C/N-TiO_2(600) hybrid shells. Fig. 10b shows the comparison of fluorescence intensity for different samples at a fixed time (30 min). As we known, the fluorescence intensity is related to the amount of produced $^{\bullet}OH$. It can be clearly seen that C/N-TiO_2(600) hybrid shells show the highest amount of $^{\bullet}OH$ radicals. It is further indicating the sample C/N-TiO_2(600) has higher photocatalytic activity than other photocatalysts. The above experiments results further confirm that $^{\bullet}OH$ radicals are active species in photocatalytic reactions. It has been indicated that the catalytic efficiency of photocatalysts mainly depends on the efficiency

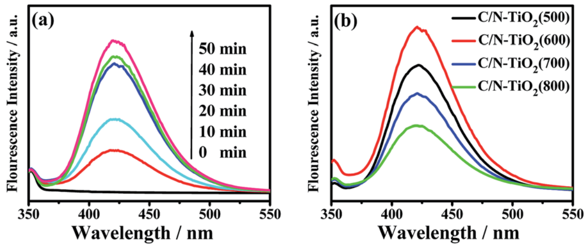

Fig. 10 (a) Fluorescence spectral changes with visible light irradiation time on C/N-TiO_2(600) hybrid shells in a 5 × 10^{-4} mol L^{-1} basic solution of terephthalic acid. (b) Fluorescence spectra of C/N-TiO_2 hybrid shells in a 5 × 10^{-4} mol L^{-1} basic solution of terephthalic acid under visible light irradiation at a fixed time of 30 min.

utilization of solar energy and the separation efficiency of the electron–hole pairs.[20] The codoping of C and N and the incorporated electrically conductive graphite carbon in TiO_2 shells are believed to contribute to light absorption and the separation efficiency of the electron–hole pairs, thereby resulting in high photocatalytic performance.

Conclusions

In summary, mesoporous C, N-codoped TiO_2 (C/N-TiO_2) hybrid shells incorporated with graphite carbon were synthesized, where PANI functioned as both C and N doping sources and supplied the graphite carbon, which can contribute to improve the visible light absorption and photogenerated electron–hole pair separation efficiency of TiO_2, and finally lead to enhanced photocatalytic activity. Results showed that C/N-TiO_2(600) hybrid shells exhibited the best overall photocatalytic activity in degradation of organic dyes and H_2 production under visible light irradiation, which could be attributed to the enhanced visible light absorption and charge separation efficiency associated with the codoped-C and N and the presence of graphite carbon. The strategy provided here will provide a promising route for the construction of other C/N-semiconductor hybrid shells for broader applications.

Acknowledgements

The authors gratefully acknowledge financial support from the National Natural Science Foundation of China (21673202 and 21273004), Innovation Program for Graduate Students in Universities of Jiangsu Province (No. KYZZ15_0361), Excellent Doctoral Dissertation of Yangzhou University, Qing Lan Project and the Priority Academic Program Development of Jiangsu Higher Education Institutions. We would also like to acknowledge the technical support received at the Testing Center of Yangzhou University.

Notes and references

1 (*a*) J. S. Lee, K. H. You and C. B. Park, *Adv. Mater.*, 2012, **24**, 1084–1088; (*b*) J. F. Ye, W. Liu, J. G. Cai, S. Chen, X. W. Zhao, H. G. Zhou and L. M. Qi, *J. Am. Chem. Soc.*, 2011, **133**, 933–940; (*c*) W. G. Tu, Y. Zhou, Q. Liu, Z. P. Tian, J. Gao, X. Y. Chen, H. T. Zhang, J. G. Liu and Z. G. Zou, *Adv. Funct. Mater.*, 2012, **22**, 1215–1221; (*d*) J. B. Joo, Q. Zhang, I. Lee, M. Dahl, F. Zaera and Y. D. Yin, *Adv. Funct. Mater.*, 2012, **22**, 166–174; (*e*) J. Du, X. Y. Lai, N. L. Yang, J. Zhai, D. Kisailus, F. B. Su, D. Wang and L. Jiang, *ACS Nano*, 2011, **5**, 590–596.

2 (*a*) J. Du, X. Y. Lai, N. L. Yang, J. Zhai, D. Kisailus, F. B. Su, D. Wang and L. Jiang, *ACS Nano*, 2011, **5**, 590–596; (*b*) M. A. Henderson and I. Lyubinetsky, *Chem. Rev.*, 2013, **113**, 4428–4455; (*c*) A. Kudo and Y. Miseki, *Chem. Soc. Rev.*, 2009, **38**, 253–278.

3 (*a*) M. Batzill, *Energy Environ. Sci.*, 2011, **4**, 3275–3286; (*b*) T. Fröschl, U. Hörmann, P. Kubiak, G. Kučerová, M. Pfanzelt, C. K. Weiss, R. J. Behm, N. Hüsing, U. Kaiser, K. Landfester and M. Wohlfahrt-Mehrens, *Chem. Soc. Rev.*, 2012, **41**, 5313–5360; (*c*) W. Zhao, W. Ma, C. Chen, J. C. Zhao and Z. Shuai, *J. Am. Chem. Soc.*, 2004, **126**, 4782–4873.

4 (*a*) Q. Zhang, D. Q. Lima, I. Lee, F. Zaera, M. F. Chi and Y. D. Yin, *Angew. Chem., Int. Ed.*, 2011, **50**, 7088–7092; (*b*) M. M. Khan, S. A. Ansari, M. I. Amal, J. Lee and M. H. Cho, *Nanoscale*, 2013, **5**, 4427–4435; (*c*) Z. Wu, Y. Y. Wang, L. Sun, Y. X. Mao, M. Y. Wang and C. J. Lin, *J. Mater. Chem. A*, 2014, **2**, 8223–8229; (*d*) M. G. Wang, J. Han, H. X. Xiong, R. Guo and Y. D. Yin, *ACS Appl. Mater. Interfaces*, 2015, **7**, 6909–6918; (*e*) M. G. Wang, Y. M. Hu, J. Han, R. Guo, H. X. Xiong and Y. D. Yin, *J. Mater. Chem. A*, 2015, **3**, 20727–20735; (*f*) J. S. Lee, K. H. You and C. B. Park, *Adv. Mater.*, 2012, **24**, 1084–1088; (*g*) B. Rico-Oller, A. Boudjemaa, H. Bahruji, M. Kebir, S. Prashar, K. Bachari, M. Fajardo and S. Gómez-Ruiz, *Sci. Total Environ.*, 2016, **563–564**, 921–932.

5 (*a*) J. H. Park, S. Kim and A. J. Bard, *Nano Lett.*, 2006, **6**, 24–28; (*b*) X. B. Chen and C. Burda, *J. Am. Chem. Soc.*, 2008, **130**, 5018–5019; (*c*) J. H. Pan, X. W. Zhang, A. J. H. Du, D. D. Sun and J. O. Leckie, *J. Am. Chem. Soc.*, 2008, **130**, 11256–11257; (*d*) W. Ho, J. C. Yu and S. Lee, *Chem. Commun.*, 2006, 1115–1117; (*e*) R. Asahi, T. Morikawa, T. Ohwaki, K. Aoki and Y. Taga, *Science*, 2001, **293**, 269–271; (*f*) S. In, A. Orlov, R. Berg, F. García, S. P. Jimenez, M. S. Tikhov, D. S. Wright and R. M. Lambert, *J. Am. Chem. Soc.*, 2007, **129**, 13790–13791; (*g*) M. Sathish, B. Viswanathan, R. P. Viswanath and C. S. Gopinath, *Chem. Mater.*, 2005, **17**, 6349–6353; (*h*) H. P. Li, W. Zhang, S. Y. Huang and W. Pan, *Nanoscale*, 2012, **4**, 801–806; (*i*) S. Lázaro-Navas, S. Prashar, M. Fajardo and S. GÓmez-Ruiz, *J. Nanopart. Res.*, 2015, **17**, 94–105.

6 (*a*) B. C. Qiu, C. C. Zhong, M. Y. Xing and J. L. Zhang, *RSC Adv.*, 2015, **5**, 17802–17808; (*b*) J. D. Zhuang, Q. F. Tian, H. Zhou, Q. Liu, P. Liu and H. M. Zhong, *J. Mater. Chem.*, 2012, **22**, 7036–7042; (*c*) G. G. Liu, F. He, J. Zhang, L. J. Li, F. J. Lia, L. X. Chen and Y. Huang, *Appl. Catal., B*, 2014, **150–151**, 515–522.

7 (*a*) S. A. Ansari, M. M. Khan, M. O. Ansari and M. H. Cho, *New J. Chem.*, 2016, **40**, 3000–3009; (*b*) Z. F. Jiang, X. M. Lv, D. L. Jiang, J. M. Xie and D. J. Mao, *J. Mater. Chem. A*, 2013,

1, 14963–14972; (*c*) D. M. Chen, Z. Y. Jiang, J. Q. Geng, Q. Wang and D. Yang, *Ind. Eng. Chem. Res.*, 2007, **46**, 2741–2746.

8 (*a*) R. Silva, D. Voiry, M. Chhowalla and T. Asefa, *J. Am. Chem. Soc.*, 2013, **135**, 7823–7826; (*b*) W. Ding, L. Li, K. Xiong, Y. Wang, W. Li, Y. Nie, S. Chen, X. Q. Qi and Z. D. Wei, *J. Am. Chem. Soc.*, 2015, **137**, 5414–5420; (*c*) S. Y. Cao, N. Han, J. Han, Y. M. Hu, L. Fan, C. Q. Zhou and R. Guo, *ACS Appl. Mater. Interfaces*, 2016, **8**, 6040–6050.

9 (*a*) M. Sathish, B. Viswanathan, R. P. Viswanath and C. S. Gopinath, *Chem. Mater.*, 2005, **17**, 6349–6353; (*b*) Y. Cong, J. J. Zhang, F. Chen and M. Anpo, *J. Phys. Chem. C*, 2007, **111**, 6976–6982; (*c*) Y. Q. Cao, T. He, Y. M. Chen and Y. A. Cao, *J. Phys. Chem. C*, 2010, **114**, 3627–3633; (*d*) Y. L. Kuo, T. L. Su, F. C. Kung and T. J. Wu, *J. Hazard. Mater.*, 2011, **190**, 938–944.

10 M. G. Wang, J. Han, Y. M. Hu, R. Guo and Y. D. Yin, *ACS Appl. Mater. Interfaces*, 2016, **8**, 29511–29521.

11 (*a*) J. Q. Shan, Y. X. Liu, P. Liu, Y. S. Huang, Y. Z. Su, D. Q. Wu and X. L. Feng, *J. Mater. Chem. A*, 2015, **3**, 24148–24154; (*b*) A. L. M. Reddy, A. Srivastava, S. R. Gowda, H. Gullapalli, M. Dubey and P. M. Ajayan, *ACS Nano*, 2010, **4**, 6337–6342; (*c*) L. L. Tian, X. Y. Wei, Q. C. Zhuang, C. H. Jiang, C. Wu, G. Y. Ma, X. Zhao, Z. M. Zong and S. G. Sun, *Nanoscale*, 2014, **6**, 6075–6083; (*d*) G. A. Ferrero, K. Preuss, A. Marinovic, A. B. Jorge, N. Mansor, D. J. L. Brett, A. B. Fuertes, M. Sevilla and M. M. Titirici, *ACS Nano*, 2016, **10**, 5922–5932.

12 (*a*) J. B. Cai, X. Q. Wu, S. X. Li, F. Y. Zheng, L. C. Zhu and Z. H. Lai, *ACS Appl. Mater. Interfaces*, 2015, **7**, 3764–3772; (*b*) M. G. Wang, J. Han, H. X. Xiong and R. Guo, *Langmuir*, 2015, **31**, 6220–6228; (*c*) M. S. A. S. Shah, A. R. Park, K. Zhang, J. H. Park and P. J. Yoo, *ACS Appl. Mater. Interfaces*, 2012, **4**, 3893–3901.

13 (*a*) M. Y. Li, Y. Hu, S. L. Xie, Y. C. Huang, Y. X. Tong and X. H. Lu, *Chem. Commun.*, 2014, **50**, 4341–4343; (*b*) J. Zheng, L. Liu, G. B. Ji, Q. F. Yang, L. R. Zheng and J. Zhang, *ACS Appl. Mater. Interfaces*, 2016, **8**, 20074–20081.

14 (*a*) S. W. Liu, J. G. Yu and M. Jaroniec, *J. Am. Chem. Soc.*, 2010, **132**, 11914–11916; (*b*) J. G. Yu and J. R. Ran, *Energy Environ. Sci.*, 2011, **4**, 1364–1371.

15 (*a*) Y. Y. Wen, H. M. Ding and Y. K. Shan, *Nanoscale*, 2011, **3**, 4411–4417; (*b*) Y. Wang, J. G. Yu, W. Xiao and Q. Li, *J. Mater. Chem. A*, 2014, **2**, 3847–3855.

16 (*a*) F. S. Wen, H. Hou, J. Y. Xiang, X. Y. Zhang, Z. B. Su, S. J. Yuan and Z. Y. Liu, *Carbon*, 2015, **89**, 372–377; (*b*) J. Q. Shan, Y. X. Liu, P. Liu, Y. S. Huang, Y. Z. Su, D. Q. Wu and X. L. Feng, *J. Mater. Chem. A*, 2015, **3**, 24148–24154.

17 (*a*) M. Q. Yang, B. Weng and Y. J. Xu, *Langmuir*, 2013, **29**, 10549–10558; (*b*) N. Zhang, Y. Zhang, X. Pan, M. Q. Yang and Y. J. Xu, *J. Phys. Chem. C*, 2012, **116**, 18023–18031; (*c*) L. Jing, Z. Y. Ynag, Y. F. Zhao, X. Guo, Y. M. Yan and K. N. Sun, *J. Mater. Chem. A*, 2014, **2**, 1068–1075; (*d*) N. Zhang, Y. H. Zhang, X. Y. Pan, X. Z. Fu, S. Q. Liu and Y. J. Xu, *J. Phys. Chem. C*, 2011, **115**, 23501–23511.

18 (*a*) J. Fernandez, J. Bandara, A. Lopez, P. Buffat and J. Kiwi, *Langmuir*, 1999, **15**, 185–192; (*b*) J. G. Yu, G. P. Dai and B. B. Huang, *J. Phys. Chem. C*, 2009, **113**, 16394–16401.

19 (*a*) K. Ishibashi, A. Fujishima, T. Watanabe and K. Hashimoto, *Electrochem. Commun.*, 2000, **2**, 207–210; (*b*) Q. Xiao, Z. C. Si, J. Zhang, C. Xiao and X. K. Tan, *J. Hazard. Mater.*, 2008, **150**, 62–67; (*c*) J. G. Yu, W. G. Wang, B. Cheng and B. L. Su, *J. Phys. Chem. C*, 2009, **113**, 6743–6750.

20 (*a*) Y. Y. Wen, H. M. Ding and Y. K. Shan, *Nanoscale*, 2011, **3**, 4411–4417; (*b*) Q. Zhang, D. Q. Lima, I. Lee, F. Zaera, M. F. Chi and Y. D. Yin, *Angew. Chem., Int. Ed.*, 2011, **50**, 7088–7092; (*c*) X. Li, X. Chen, H. Niu, X. Han, T. Zhang, J. Y. Liu, H. M. Lin and F. Y. Qu, *J. Colloid Interface Sci.*, 2015, **452**, 89–97; (*d*) Z. Wu, Y. Y. Wang, L. Sun, Y. X. Mao, M. Y. Wang and C. J. Lin, *J. Mater. Chem. A*, 2014, **2**, 8223–8229.